Solute-defect interactions in Al-Mg alloys from diffusive variational Gaussian calculations

E. Dontsova,[1,*] J. Rottler,[2] and C. W. Sinclair[1]

[1]*Department of Materials Engineering, The University of British Columbia, Vancouver, British Columbia, Canada V6T 1Z4*

[2]*Department of Physics and Astronomy, The University of British Columbia, Vancouver, British Columbia, Canada V6T 1Z1*

(Received 29 July 2014; revised manuscript received 16 October 2014; published 5 November 2014)

Resolving atomic-scale defect topologies and energetics with accurate atomistic interaction models provides access to the nonlinear phenomena inherent at atomic length and time scales. Coarse graining the dynamics of such simulations to look at the migration of, e.g., solute atoms, while retaining the rich atomic-scale detail required to properly describe defects, is a particular challenge. In this paper, we present an adaptation of the recently developed "diffusive molecular dynamics" model to describe the energetics and kinetics of binary alloys on diffusive time scales. The potential of the technique is illustrated by applying it to the classic problems of solute segregation to a planar boundary (stacking fault) and edge dislocation in the Al-Mg system. Our approach provides fully dynamical solutions in situations with an evolving energy landscape in a computationally efficient way, where atomistic kinetic Monte Carlo simulations are difficult or impractical to perform.

DOI: 10.1103/PhysRevB.90.174102 PACS number(s): 66.30.−h, 64.75.Op, 61.72.Lk

I. INTRODUCTION

Solute-defect interactions in crystalline materials are used to manipulate the local chemistry of surfaces and dislocations to achieve desirable functional and mechanical properties [1,2]. Technologically, solute segregation to surfaces is used to modify properties as diverse as the catalytic response of nanoparticles (e.g., [3]), the creep resistance of ceramics (e.g., [4]) and the strength of structural alloys (e.g., [5,6]). While phenomenological models for segregation-based processes exist, attempts at quantitative prediction often suffer from insufficient knowledge of the many possible atomic-scale solute-defect interactions. In this case, one would like to link atomic-scale information to continuum models thereby improving our predictive capabilities. An example of how this approach can be successfully applied to enumerate continuum models and identify new, previously unidentified, mechanisms is the recent achievement in predicting dynamic strain aging [7–9] in Al-Mg alloys [10–15].

It remains, however, a significant challenge to capture in a single, self-consistent model, both the atomistic nature of solute-defect interaction and the diffusive time scale of solute redistribution. For problems such as the one described above, the requirement for diffusive time scales makes simulation impossible with standard molecular dynamics (MD) methods. At the same time, purely continuum models are inappropriate near defects where atomistic details become important. For the computation of equilibrium solute concentration profiles at grain boundaries and interfaces, a common strategy is to obtain binding energies from an atomistic model and use those in conjunction with adsorption models such as the Langmuir-McLean model [16]. This approach, however, neglects interactions between solute atoms and is only accurate in the dilute limit. These limitations can in principle be lifted by performing fully atomistic equilibrium Monte Carlo (MC) simulations [11,12], Foiles' study of segregation to grain boundaries being an early example of this approach [17]. Such MC simulations are much more computationally intensive and become particularly difficult when large strain energy gradients are present. If information about kinetics is needed, one may resort to a kinetic MC treatment, but this requires precomputation of activation barriers that is no longer tractable for most problems when long-ranged interactions are present.

In this work, we introduce an alternative approach that provides access to diffusive time scales but retains crucial features at atomic length scales. The method can be viewed as a dynamical version of the variational Gaussian (VG) method [18,19] that was recently extended by Li *et al.* [20] to include vacancy dynamics. Here, atoms are represented by continuous density fields whose time evolution is governed by a Helmholtz free energy in combination with first-order relaxation kinetics. The approach has been called "diffusive molecular dynamics" (DMD), but the dynamics evolves the mass density field and not individual particle trajectories from equations of motion. As a result, the description is now "phonon free" in the sense that lattice vibrations are no longer explicitly followed as in MD. The characteristic dynamical time scale is therefore $\tau \sim a_0^2/D$, where a_0 and D are the lattice and diffusion constants, respectively. The method provides a good starting point to investigate vacancy mediated transport phenomena, for instance, dislocation climb [21].

The DMD approach shares with classic phase field models the representation of matter as a continuous density field evolving on diffusive time scales. However, it goes beyond a phase field description by including distinct atomistic features such as discrete representation of interfaces and defects with long-ranged elastic fields driving mass transport. This level of description is akin to a kinetic MC simulation, but the latter has the potential for a more accurate description of migration barriers.

Here, we present a generalization of the DMD method to binary alloys, using the well-characterized Al-Mg system to illustrate some of the strengths of this approach. We first show that static finite-temperature properties such as free energies and elastic constants can be very efficiently computed using the variational Gaussian approach. We then apply the dynamical formulation to simulate segregation of Mg towards two different types of defects in fcc Al. First, results are presented for the segregation to a stacking fault, where the

*Corresponding author: evgeniya.dontsova@ubc.ca

driving force for solute redistribution is purely chemical. Following this, segregation to a split edge dislocation is used to illustrate the case where both short-range chemical and long-range elastic interactions determine the kinetics and equilibrium segregation. In both cases, we find qualitative agreement with, but quantitative deviations from, continuum segregation models. At higher concentrations, our calculations predict the formation of an ordered intermetallic precipitate at the core of the dislocation, an intrinsically atomistic effect beyond the reach of continuum models.

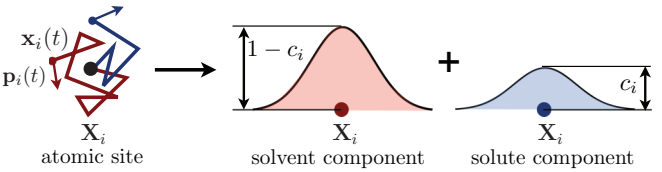

FIG. 1. (Color online) Schematics of the main approximations used in the DMD approach for binary alloys. Solvent and solute atoms (shown in different colors) undergoing thermal vibrations around the same position $\mathbf{X}_i$ in MD (left) are represented in DMD by superposition of Gaussians (right) for each atomic species at this atomic site.

II. METHODOLOGY

Widely used to model materials at the atomic scale, MD can not be applied to most diffusional problems because the integration time step is constrained by the vibrational frequencies. However, most of the time atoms in solids at finite temperature vibrate around their mean positions. Generally, such fluctuations occur in a narrow region, and hence in a harmonic approximation, the atomic positions can be represented by Gaussian density clouds (see Fig. 1). In other words, the finite-temperature effects can be captured by associating an atom with its mean position $\mathbf{X}_i$ and the width of a Gaussian that reflects the magnitude of thermal vibrations. The Gaussian width $\sigma = 1/\sqrt{2\alpha_i}$ can be related to $\alpha_i = m_i\omega_i^2/(2k_BT)$, where m_i is an atomic mass, ω_i is a vibrational frequency, k_B is the Boltzmann constant, and T is the absolute temperature. Optimization of these parameters $\{\mathbf{X}_i,\alpha_i\}$ for $i = 1,2,\ldots,N$, where N is the number of atoms, by minimizing the Helmholtz free energy provides the basis of the VG method originally introduced by LeSar *et al.* [18]. Therefore, VG calculations can be viewed as an efficient way to predict an equilibrium structure at finite temperature. However, as a purely minimization technique it cannot provide any information about the kinetics of a process.

For this reason, the VG method was extended in the DMD method [20] to capture the time evolution of a pure metal containing mobile vacancies. Aside from the mean position and Gaussian width, each site is now also assigned an occupation probability that reflects the probability of being occupied by an atom rather than a vacancy. Time evolution of the vacancy field is achieved in two steps. First, the Gaussian mean positions and widths are optimized by minimizing the Helmholtz free energy. Second, the occupation probabilities are computed by solving a system of rate equations. This assumes that atomic positions relax much faster than any chemical potential gradients arising from the vacancies. These steps are iterated, this amounting to the solution of a diffusion problem on an irregular lattice where local fluxes are resolved at the atomic scale.

In this model, the flux of vacancies is determined by the local spatial variation in the vacancy concentration field. In many problems of interest (see, e.g., [20,21]) the energetics of the system drive vacancies to localize. Such localization leads to very steep gradients in energy between neighboring atomic sites and a necessarily slowing down of the DMD dynamics. Indeed, in the worst case when a realistic (low) average vacancy concentration is used in a simulation where strong vacancy localization occurs, the integration time step required approaches that used in MD simulations and the kinetic advantages of the technique disappear.

In our generalization to binary alloys, this difficulty is averted by the fact that (i) real systems of interest have much larger solute concentrations than vacancy concentrations and (ii) solution thermodynamics tends to predict phases that have mutual solubility. In developing this alloy DMD model each atomic site is assigned an occupation probability denoted by c_i, this indicating the relative site concentration of each atomic species. By convention, a site with $c_i = 1$ is considered to be occupied purely by a solute Mg atom, while $c_i = 0$ corresponds to a solvent Al atom. The main approximations behind the DMD approach for binary alloys are shown schematically in Fig. 1.

In analogy with Eq. (3) in [20], we write the variational Gaussian Helmholtz energy for an A-B binary alloy described by an embedded-atom method (EAM) potential as

$$F = \frac{1}{2}\sum_{i=1}^{N}\sum_{j\neq i}\{c_ic_jw_{AA}(X_{ij},\alpha_{ij}) + [c_i(1-c_j) + (1-c_i)c_j]w_{AB}(X_{ij},\alpha_{ij}) + (1-c_i)(1-c_j)w_{BB}(X_{ij},\alpha_{ij})\}$$
$$+ \sum_{i=1}^{N}[c_iE_A(\bar{\psi}_i) + (1-c_i)E_B(\bar{\psi}_i)] + \frac{3}{2}k_BT\sum_{i=1}^{N}\left[\ln\left(\frac{\alpha_i\Lambda_T^2}{\pi}\right) - 1\right] + k_BT\sum_{i=1}^{N}[c_i\ln c_i + (1-c_i)\ln(1-c_i)]. \quad (1)$$

The first terms correspond to the energetic contributions arising from the EAM potential, while the last two terms reflect the vibrational and configurational entropy. In the present description, the configurational alloy thermodynamics is treated at the pairwise level as in the underlying EAM potential, the vibrational contribution of free energy is harmonic approximation of an Einstein solid with a single frequency for each atom, and configurational entropy is the standard entropy of mixing. Here, $\bar{\psi}_i = \sum_{j\neq i}[c_j\psi_A(X_{ij},\alpha_{ij}) + (1-c_j)\psi_B(X_{ij},\alpha_{ij})]$, the functions w_{IJ} and ψ_I are the Gaussian averaged pair

potential and electronic density, E_I is the EAM embedding function, $\alpha_{ij} = (\alpha_i^{-1} + \alpha_j^{-1})^{-1}$, $X_{ij} = |\mathbf{X}_i - \mathbf{X}_j|$, and $\Lambda_T = \hbar\sqrt{2\pi/(m_i k_B T)}$ is the thermal de Broglie wavelength. The Gaussian averaging can be viewed as "thermalizing" the EAM potential by integrating pair potential and electronic density with two interacting Gaussians within the cutoff region, as described in [20]. It is important to note that the Helmholtz free energy given by Eq. (1) is an upper bound estimate of the true Helmholtz free energy based on the Gibbs-Bogoliubov inequality [18,19]. The accuracy of Eq. (1) was confirmed by comparing free energies and volume per atom for Cu with nominally exact MC simulations over a wide temperature range in [18] and with direct molecular dynamics in [20]. While these two quantities show excellent agreement with truly atomistic calculations, the rms vibrational amplitudes tend to be underestimated by VG.

In this work, we have used the EAM potential for the Al-Mg system developed by Liu *et al.* [22], although in principle any binary alloy EAM potential can be used with the technique described above. The Liu Al-Mg potential has been used extensively in the past, particularly for studying solute-defect interactions in dilute ($\leqslant$10 at.% Mg) Al-Mg alloys [10–12,14], this being the composition range of technologically important, solid solution strengthened 5XXX alloys.

Diffusion of solute in this model does not explicitly involve vacancies. Rather, the time evolution of the solute concentration field c_i is assumed to be governed by the following system of rate equations:

$$\frac{dc_i}{dt} = \frac{1}{8\pi\tau}\sum_j{}' \left[c_j(1-c_i)\exp\left(-\frac{f_{ij}}{2k_BT}\right) - c_i(1-c_j)\exp\left(\frac{f_{ij}}{2k_BT}\right)\right], \quad (2)$$

where the primed summation is made over diffusing neighbors. The formation energy at an atomic site f_i is given by the derivative of the free energy with respect to c_i minus the configurational entropy. The local effect of atomic structure on solute redistribution in Eq. (2) is then incorporated through $f_{ij} = f_i - f_j$, the difference in formation energy between two adjacent sites. The characteristic diffusion time scale is $\tau = a_0^2/(8\pi D)$, where a_0 is the fcc lattice constant, $D = D_0 \exp(-Q_d/k_BT)$ is the diffusivity of Mg in Al with a pre-exponential factor $D_0 = 1.2 \times 10^{-4}$ m^2/s, and the activation energy for diffusion $Q_d = 1.35$ eV/atom [23]. With these values, $\tau = 12\,\mu$s at $T = 600$ K. Equation (2) is motivated from an atomistic treatment of jump processes and consistent with continuum diffusion in the long-time limit. Local jump rates depend on local composition via the formation energy difference between the adjacent sites.

The DMD method is developed in the grand canonical (μVT) ensemble, allowing exchange of mass between the simulation domain and an infinitely large reservoir of solute. The grand potential for the binary alloy system

$$\Omega = F - \Delta\mu \sum_{i=1}^{N} c_i, \quad (3)$$

with $\Delta\mu = \mu_{\mathrm{Mg}} - \mu_{\mathrm{Al}}$ being the chemical potential difference between atomic species in the reservoir, is minimized at each step. In practice, this reservoir is connected to the simulation domain by introducing a fixed composition to a layer of atoms at the boundary of the simulation domain. Solving the diffusion equation (2) then allows solute to flow in or out of the system through this boundary. Alternatively, if the boundary atom compositions are not fixed, then the number of solute atoms in the system is fixed and the simulation can be considered to be in a canonical (NVT) ensemble.

III. RESULTS AND DISCUSSION

A. Finite-temperature properties

The above framework provides a fast and efficient way to compute the Helmholtz energy compared with more computationally intense methods such as quasiharmonic theory (VG belongs to a classical limit of this model) and thermodynamic integration. Calculations were performed to compute the VG Helmholtz free energy starting from a uniform solid solution (each site having the same value of c_i) in a perfect fcc crystal containing 16 atoms. The Helmholtz free energy given in Eq. (1) was minimized with respect to atomic position and Gaussian widths while the site concentrations were kept constant. The calculations were performed in the NVT ensemble with a volume that corresponded to a negligible hydrostatic pressure (<1 MPa). Figure 2 shows the VG result for the mixing enthalpy $\Delta H_{\mathrm{mix}} = H - [(1-c_0)H_{\mathrm{Al}} + c_0 H_{\mathrm{Mg}}]$ and free energy $\Delta F_{\mathrm{mix}} = \Delta H_{\mathrm{mix}} - T\Delta S_{\mathrm{mix}}$ of the Al-Mg solid solution as a function of the average solute concentration, denoted by c_0, for different temperatures. All mixing quantities are calculated in a similar manner. The mixing enthalpy varies only weakly with temperature, while ΔF_{mix} varies strongly and predicts demixing at low temperatures. Comparison of the VG predictions with conventional molecular statics (MS) calculations [also shown in Fig. 2(a)] averaged over 10 different configurations of the random solid solution confirms that the peculiar shape of the enthalpy of mixing is given almost purely by the EAM potential. We also show a comparison with experimentally evaluated CALPHAD data [24]. While the enthalpy of mixing exhibits deviations from the CALPHAD predictions especially at higher concentrations and does not preserve the shape over a wide composition range, the EAM potential still captures the general trend at the lower solute

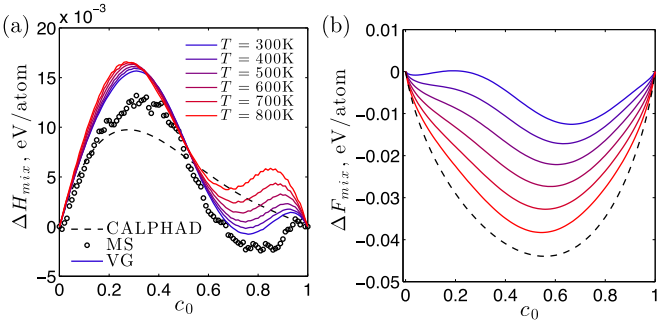

FIG. 2. (Color online) (a) Enthalpy and (b) free energy of mixing versus Mg solute concentration c_0 given by VG calculations for Al-Mg solid solution (with fcc Mg) at different temperatures. Here, MS data correspond to properties at $T = 0$ and the CALPHAD data at $T = 800$ K.

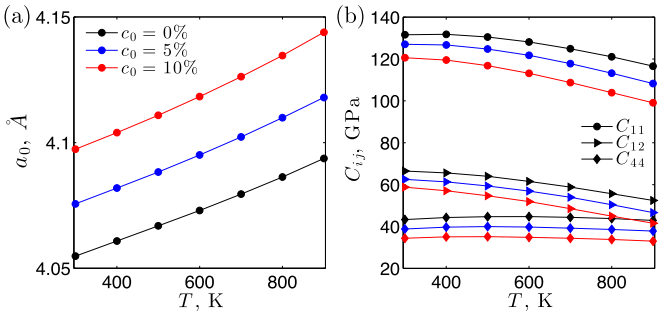

FIG. 3. (Color online) Temperature dependence of (a) lattice constant and (b) elastic constants of Al-Mg alloy for different compositions obtained by DMD method.

concentrations of interest here (the highest concentration in the segregation calculations is about 30% Mg).

The same set of calculations also provides us with an estimate of the lattice constant and the elastic constants of the Al-Mg solid solutions versus temperature T. These results are shown in Fig. 3 for three different alloy compositions 0%, 5%, and 10% Mg. The lattice constant increases almost linearly with temperature and Mg concentration in agreement with expectations [25].

The present EAM potential predicts a softening of C_{11} and C_{12} with increasing temperature, while C_{44} is essentially constant, in agreement with experiments and first-principles calculations on pure Al [26]. All elastic constants decrease with increasing Mg concentrations, which is consistent with the results obtained by using the MC method and the same EAM potential and presented in [13]. The latter predicts about 10% higher reduction in C_{11} and C_{12} constants and no difference for C_{44} with increase in Mg content in comparison with our data at $T = 0$.

B. Segregation towards a stacking fault

A stacking fault (SF) was created by removing one {111} plane in a periodic simulation box having dimensions of $5.8 \times 430 \times 10$ Å^3 along the $[1\bar{1}0] \times [111] \times [\bar{1}\bar{1}2]$ directions, the simulation box containing 1456 atoms. Next, an average solute concentration c_0 was assigned to every atomic site, meaning that solute was evenly distributed in the matrix. The simulation box dimensions were adjusted so that all stress components on the box were near zero (<1 MPa). Finally, this structure was used as the initial condition for a DMD calculation in the NVT ensemble at $T = 600$ K. Simulations performed at other temperatures showed all of the same physics as those shown here.

Figure 4 shows the solute distribution in the vicinity of the SF for three different solute concentrations $c_0 = 1\%$, 5%, and 10% after a time sufficient to reach equilibrium. The segregation of Mg towards the stacking fault is not surprising given that the hcp structure is energetically more favorable than the fcc structure for pure Mg. This is consistent with VG calculations that showed the stacking fault energy (SFE) decreasing by 20% between pure Al and Al-20 at.% Mg. As can be seen from Fig. 4, the two atomic planes straddling the SF have the highest Mg concentration, the profile being limited to the three atomic planes on either side of the SF.

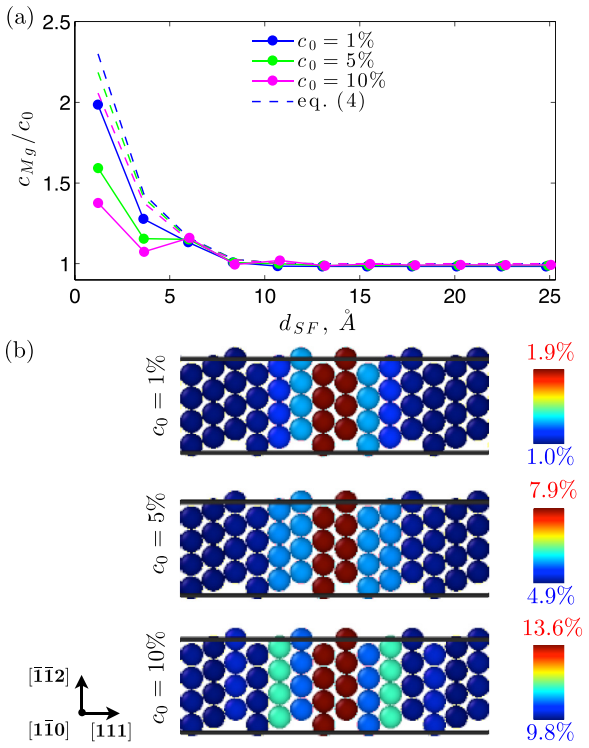

FIG. 4. (Color online) (a) Plot of solute concentration normalized by the initial concentration c_0 versus the distance to SF, d_{SF}, at $T = 600$ K. (b) Atomistic representation of solute distribution near the SF defect depicted by highest solute concentration.

If one assumes thermodynamic equilibrium and neglects interactions between solute atoms, the concentration of solute in the vicinity of a defect can be predicted by the following expression:

$$c(\mathbf{r}) = \frac{1}{1 + \frac{1-c_0}{c_0} \exp\left(\frac{U(\mathbf{r})}{k_B T}\right)}, \tag{4}$$

where $U(\mathbf{r})$ is a spatially varying binding energy between the solute atom and defect. In the case of the SF the binding energy can be easily calculated with static VG minimization. A comparison between the full DMD solute segregation profile and the prediction of Eq. (4) is given in Fig. 4(a) for the present system at 600 K. The agreement is better for smaller solute concentration, while for higher concentrations solute-solute interactions become important. In particular, in the case of $c_0 = 10\%$ the effect of Mg-Mg repulsion is more pronounced near the SF, i.e., oscillatory behavior of solute concentration can be observed for a few planes close to the SF. Previous atomistic MC calculations on the same Al-Mg system with the same EAM potential [12] also suggest that above $c_0 = 6\%$, solute-solute interactions become more important and the accuracy of Eq. (4) diminishes near the defect.

Figure 5(a) shows the time evolution of a normalized solute concentration at the SF. For interfacial segregation, the continuum diffusion model by McLean [16] provides the following analytical prediction:

$$\frac{c_{\mathrm{Mg}}(t) - c_0}{c_{\mathrm{Mg}}(\infty) - c_0} = 1 - \exp(s^2)\mathrm{erfc}(s), \tag{5}$$

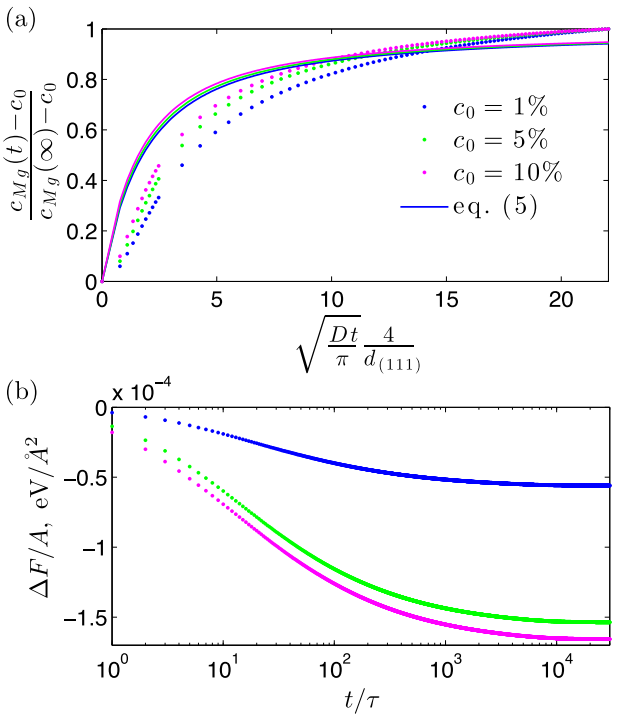

FIG. 5. (Color online) Time evolution of (a) the solute concentration of atoms located in the SF planes and (b) free-energy difference between the current and initial states per SF area for $c_0 = 1\%$, 5%, and 10% at $T = 600$ K from NVT DMD calculations.

where $s = \sqrt{Dt}/(\beta d_{(111)}/2)$ and β describes the solute enrichment at the defect relative to the bulk. In general, this enrichment factor changes dynamically throughout the segregation process, but in order to use Eq. (5) analytically β must be assumed constant. Predictions from Eq. (5) using $\beta = c_{\mathrm{Mg}}(\infty)/c_0$ can be compared with the full DMD results in Fig. 5(a). Both theory and simulations exhibit $\sqrt{t}$ behavior at short times, but the analytical model rises almost three times faster because the equilibrium value of β underestimates its true value at short times. In the long-time limit [not shown in Fig. 5(a)], all curves converge to one as they reach saturation, but quantitative differences remain for all intermediate times. The increase in solute concentration at the boundary occurs simultaneously with a decrease in system free energy due to the relaxational dynamics. Figure 5(b) shows the free-energy difference per SF area A with respect to the initial condition $\Delta F/A = F/A - F/A|_{t=0}$ over the entire simulation, including the equilibration regime when $\partial(\Delta F/A)/\partial t = 0$. Together these results illustrate that DMD captures all basic elements of the diffusional process correctly, but arrives at quantitatively different predictions by including effects that are not present in the continuum model.

C. Segregation towards a split edge dislocation

The segregation of substitutional solute to the elastic field of a split edge dislocation is a classic problem that has been treated using analytical models (e.g.. [27,28]), Metropolis MC simulations [11] and energy minimization based on the VG approximation [29]. Attempts at capturing the kinetics of segregation, where kinetic MC is the only available tool, are always hindered by the need to compute barriers which are necessarily changing during the progress of the simulation [10]. In this case, it is typical to use precomputed barriers from the starting simulation cell and to not evolve these during the simulation. The alloy DMD model described here avoids these problems.

A single edge dislocation with Burgers vector $\mathbf{b} = \frac{a_0}{2}[1\bar{1}0]$, which splits into two partials connected by a stacking fault according to the reaction $\frac{a_0}{6}[1\bar{2}1] + \frac{a_0}{6}[2\bar{1}\bar{1}]$, was constructed by removing two $(1\bar{1}0)$ planes from an initially perfect crystal. To avoid the formation of a dislocation dipole, fixed boundaries were used in the [111] direction. Next, this structure was relaxed and the simulation box volume adjusted to minimize the external stresses. In all calculations presented in the following, the simulation box contains about 27 000 atoms with $213 \times 213 \times 10$ Å^3 dimensions along $[1\bar{1}0] \times [111] \times [\bar{1}\bar{1}2]$ directions. Convergence of the results with respect to the size of the cell was confirmed, meaning that interaction with images could be neglected.

In contrast to the SF case, solute segregation in this case is driven by the long-range stress field produced by the dislocation. We performed DMD calculations starting from a uniformly distributed solute field, the simulation continuing until the solute distribution around the dislocation reached equilibrium. Figure 6 shows the solute distribution around the dislocation core for 1% [top row, Fig. 6(a)] and 5% Al-Mg alloys [middle row, Fig. 6(b)]. The first column shows the outcome of the full DMD simulation, while the second column computes the solute distribution using Eq. (4). Here, the interaction energy is approximated by $U(\mathbf{r}) = p(\mathbf{r})\Delta v$, where $p(\mathbf{r})$ is the hydrostatic pressure field and $\Delta v = v_{\mathrm{Mg}} - v_{\mathrm{Al}}$ is the atomic volume difference between Mg and Al atoms [27]. In order to account for the effect of boundary conditions and discrete atomistic effects at the core, we obtained the atomistic virial pressures $p(\mathbf{r})$ numerically from the initial configuration where the solute was distributed uniformly rather than using the analytical continuum elasticity solution for the pressure field around a split edge dislocation. Figure 6(c) shows the difference between these two (elasticity and DMD) predicted concentration fields. As expected, differences in the predicted concentration are most pronounced near the core region, and quantitatively much more significant in the 5% case. These results parallel our findings for the SF, reflecting the increasing importance of the interactions between solute atoms with increasing concentration. The similarity to the SF case extends to the fact that the concentration field below the dislocation is not uniform in case of $c_0 = 5\%$ [Fig. 6(d)]. One sees an oscillation in the Mg concentration in the tensile region just below the dislocation, this being a consequence of the repulsive nature of the Mg-Mg interaction at close separation.

Another feature captured by the alloy DMD simulation that is not accessible to continuum simulations is the segregation-induced change in partial dislocation separation. As noted above, both the SF energy and the shear modulus (approximately C_{44} in nearly isotropic Al) decrease with increasing Mg concentration, as does the ratio of $C_{44}b^2/\gamma_{\mathrm{SF}}$. Given that this ratio is proportional to the spacing between the partial dislocations, it is expected that the separation should decrease with increasing solute segregation. Indeed, careful inspection

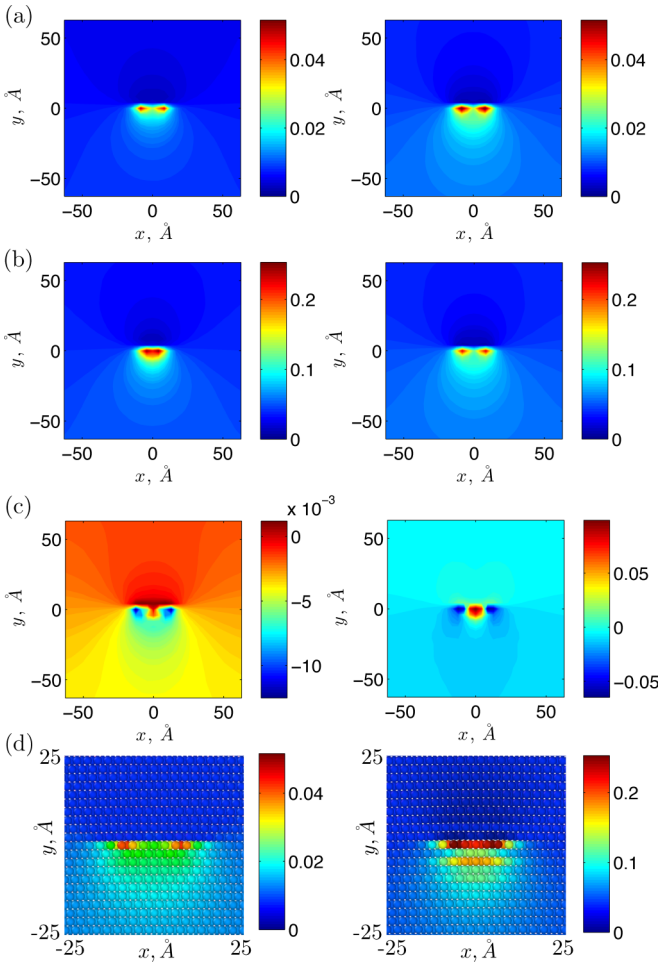

FIG. 6. (Color online) Contour plots of solute concentration near the split edge dislocation from DMD calculation (left) and from the hydrostatic pressure field existing prior to segregation (right) for (a) $c_0 = 1\%$ and (b) 5% at $T = 600$ K. (c) Contour plots of the difference between these results and (d) magnified snapshots of the concentration field illustrating the details of the solute distribution for 1% Mg (left) and 5% Mg (right).

of the left-hand panels of Figs. 6(a) and 6(b) shows a closer separation for the simulation with $c_0 = 5\%$ Mg where the magnitude of segregation is higher. Analysis of the disregistry along the slip plane for $c_0 = 5\%$ Mg shows that in this case the spacing between partials has decreased from 1.8 to 0.9 nm after segregation has completed.

In order to gain more insight into the cause of the differences in solute distributions shown in Fig. 6, we study the hydrostatic pressure field $p(\mathbf{r})$ created by the two partial dislocations in more detail. To this end, the pressure field in the initial uniform 5% alloy is shown in Fig. 7(a), while the results after equilibration with DMD in the NVT and μVT ensembles are shown in Figs. 7(b) and 7(c), respectively. For the present geometry and Burgers vector, the area above the stacking fault is under compression, while the area below is under tension. Stress relaxation in the tensile region can be observed in the equilibrated structures, which is expected due to segregation of larger Mg solute atoms in the region under tension. In the μVT ensemble, a larger Mg concentration ($\simeq$5% larger at the

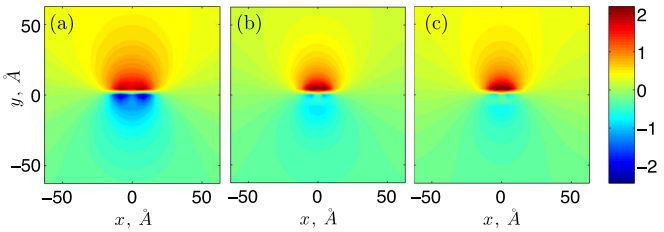

FIG. 7. (Color online) Contour plots of hydrostatic pressure fields measured in GPa near the split edge dislocation in (a) initially disordered Al-Mg solid solution, DMD relaxed structures in the (b) NVT and (c) μVT ensembles for $c_0 = 5\%$ at $T = 600$ K.

core than in the NVT ensemble) is reached at the very cores of partial dislocations which leads to even larger stress relaxation in the dilated region in comparison with NVT simulations. It is important to note that while our calculations are performed under constant volume the increase in pressure on the box during the solute segregation process is practically negligible (rising from 1 MPa for initial structure to 10 MPa for final structure). Besides, hydrostatic pressure is found to have no significant influence on Mg clustering and segregation [12].

A unique strength of the alloy DMD simulations is that they provide insight into how atomistic effects influence the kinetics of segregation. Although there is a net influx of Mg atoms towards the dislocation cores, it is useful to consider tensile and compressive regions separately. Figures 8(a) and 8(b) show the time evolution of the excess concentration $S(t)/c_0$, where

$$S(t) = \frac{1}{N_{\text{shell}}} \sum_{k=1}^{N_{\text{shell}}} [c_k(t) - c_0], \tag{6}$$

and the sum is carried out over concentric cylindrical shells [see legend of Fig. 8(b)] that contain N_{shell} atoms. For all shells, there is an outflow of Mg atoms in the compressive region and an influx in the tensile region, their magnitudes decreasing with distance from the dislocation core. In the case of the NVT ensemble shown in Fig. 8(a), a small overshoot in solute concentration is observed, which is a consequence of the fixed solute content and the finite size of the simulation box used. For the μVT ensemble shown in Fig. 8(b) the solute concentration monotonically approaches its saturation level, this level being higher than that obtained in the NVT case. Figure 8(c) shows the total change in the tensile core region ($r < R_c$) normalized by the saturation value $S(\infty)$ for the two ensembles. In this representation it is possible to compare the simulations with continuum prediction of segregation kinetics towards dislocations considering bulk diffusion rather than pipe diffusion. The Cottrell-Bilby [27] equation for segregation kinetics, modified by Louat [28] to account for saturation, is

$$\frac{S(t)}{S(\infty)} = 1 - \exp[-(t/t^\star)^{2/3}], \tag{7}$$

where

$$t^\star = \frac{\sqrt{2}b^2}{D} \frac{k_B T}{U} \left(\frac{c(\infty)}{3c_0} \right)^{3/2}. \tag{8}$$

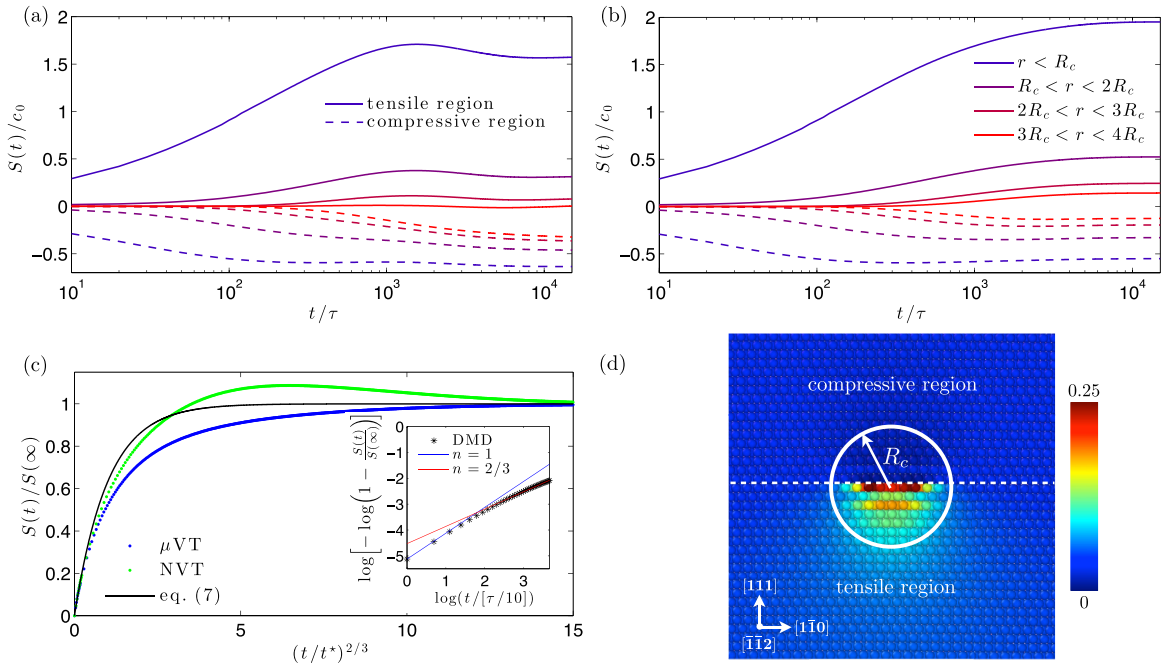

FIG. 8. (Color online) Time evolution of the solute concentration in the vicinity of the dislocation from (a) NVT and (b) μVT DMD calculations for $c_0 = 5\%$ at $T = 600$ K. (c) Comparison of the solute segregation kinetics in the tensile part of the core region [denoted by white circle with radius R_c in (d)] between different ensembles and continuum model predictions. (d) Atomic representation of solute distribution near the split edge dislocation core. The circle of radius $R_c = 13$ Å (∼distance between partials) indicates the core region.

This expression was derived under the assumption of a perfect edge dislocation and linear elasticity. In this case, $U = p\Delta v$ is the product of the pressure induced by the dislocation at a given location and the difference in atomic volume of Mg and Al, $\Delta v = v_{\mathrm{Mg}} - v_{\mathrm{Al}}$. Applying the above expression analytically therefore requires the determination of U just outside of the core of the dislocation where linear elasticity applies (e.g., at a distance between b and $1/2b$ from the center of the dislocation as assumed in [10,28]). The present atomistic simulations account for a range of binding energies making a direct comparison to Eq. (7) complicated. Rather than following the concentration evolution at a single atomic site, we have therefore followed Xu and Picu [11] and compared this expression to the value of $S(t)$ [Eq. (6)] in the tensile region contained within a half cylinder of radius R_c centered on the dislocation. Choosing to look at only the tensile region is consistent with the fact that Eq. (7) can describe only monotonic change in the solute concentration near the dislocation due to bulk diffusion, i.e., either inflow or outflow of solute atoms depending on initial conditions.

A second complication that is not naturally captured in the above model is the fact that the diffusivity is strongly modified by the stress field surrounding the dislocation. The DMD model explicitly captures this effect through the spatial variation in the formation energies [Eq. (2)]. To remain consistent with the classical application of Eq. (8) [10,28], we have used the bulk diffusivity to predict D in $t^\star$.

At short times, this analytical expression predicts $S(t)/S(\infty) \approx (t/t^\star)^{2/3}$. In this case, $t^\star$ can be determined from the initial slope of a plot of $S(t)/S(\infty)$ versus $t^{2/3}$. Figure 8 indeed shows that the initial rise of $S(t)/S(\infty)$ with time is consistent with Eq. (7), while deviations become apparent at intermediate times. It is interesting to compare the numerical values of the crossover time $t^\star$ extracted from the simulations to those predicted by Eq. (8). For this comparison one must choose a value for U. Despite the fact that at the core of the dislocation linear elasticity will not be satisfied, a first estimate was made using $p = p_{\max}$, the pressure obtained from an atomic site at the very core of the partial dislocation. Also, $c(\infty)$ was calculated from Eq. (4). From this we find the crossover time $t^\star = 25\tau$ which is roughly four times smaller than the value obtained from the initial behavior of the DMD data (Table I, labeled by NVT and μVT). Using this value of U represents an absolute upper bound to the binding energy between Mg and the dislocation. Using a value of U obtained from a site further from the dislocation core leads to an even lower predicted value for $t^\star$. For example, by using a value of U obtained from a value of p calculated as an average over sites located within $r < R$ of a tensile region centered at the dislocation leads to the values given in Table I. Thus,

TABLE I. Crossover time $t^\star$ given by Eq. (8) where an average value of the binding energy U in the tensile region of radius R has been used. Also given are the NVT and μVT DMD predicted $t^\star$; these have been found from a log-log plot of Eq. (7) where linear regression with a slope fixed at $\frac{2}{3}$ was performed. In these cases, the average composition in the region of size R has been used.

R/R_c	1.0	1.5	2.0	2.5	3.0
$t^\star/\tau$ [Eq. (8)]	13.2	13.6	14.3	15.1	16.0
$t^\star/\tau$ (NVT)	95	118	148	168	182
$t^\star/\tau$ (μVT)	134	180	249	317	386

while the continuum model appears to do a reasonably good job of predicting the time evolution of the segregation profile below the dislocation, the value of $t^\star$ is not well described by Eq. (8). On the other hand, atomistic simulations such as the ones shown here provide a way to gauge the variation of $t^\star$ for a particular system without the restrictive approximations inherent in Eq. (8).

While the continuum diffusion model does seem to contain much of the relevant physics of solute redistribution around dislocations, it misses an important aspect that becomes relevant at very short times. Due to the strong driving force for cross-core diffusion, the concentration change is initially dominated by direct atomic jumps from the compressive to the tensile region. As discussed by Curtin *et al.* [10], this mechanism implies a linear rise of the concentration with time rather than the $t^{2/3}$ behavior of Eq. (7) for times shorter than a crossover time $t_0 = 2b^2k_BT/6DU$ after which bulk diffusion dominates. The inset of Fig. 8(c) shows a magnification of this early time regime in a log-log plot. Consistent with these arguments, we find deviations from the $t^{2/3}$ dependence and a faster rise below the crossover time t_0. Our numerical value of $t_0 \approx \tau$ is about half the value predicted from the above estimate. It is impressive that our DMD alloy approach does capture this subtle but important effect, which has been argued to lie at the origin of dynamic strain aging [10].

As a final demonstration of the capabilities of the alloy DMD technique, we illustrate in Fig. 9 results obtained for an Al-Mg alloy at a higher concentration of $c_0 = 10\%$ Mg.

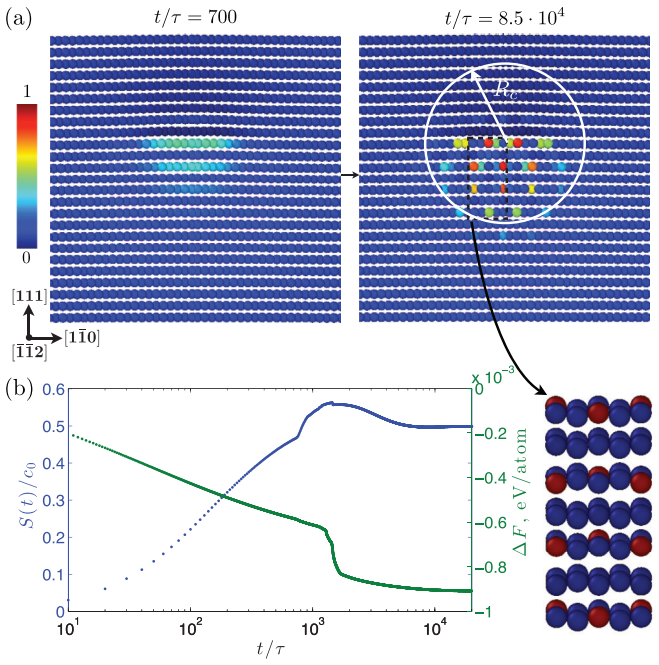

FIG. 9. (Color online) (a) Two snapshots from DMD simulations (times indicated above the figures) for solute segregation near the split edge dislocation for $c_0 = 10\%$ at $T = 600$ K. The unit cell of a fully ordered precipitate obtained from cooling this system to a lower temperature is shown at the bottom right. (b) Time evolution of the normalized excess solute concentration (blue symbols) in the region indicated by the white circle in (a) and the free-energy difference (green symbols) between the current and initial states.

As for the simulations with lower solute content, solute first accumulates near the dislocation in the form of an enriched solute field [see Fig. 9(a) left]. A sudden change occurs after a certain level of segregation, this being marked by a rapid increase in the flux of Mg [see Fig. 9(b)]. After this point, the smoothly varying concentration field rapidly transformations into an ordered phase [see Fig. 9(a) right], this transformation being accompanied by a precipitous drop in free energy [Fig. 9(b)].

Experimentally, binary Al-Mg alloys are known to form ordered $L1_2$ precipitates for $c_0 \geqslant 10\%$ Mg and long aging times at temperatures below 100 °C [30–32]. The EAM potential used here has been employed previously to examine the precipitation of $L1_2$ via kinetic MC [33], the potential having originally been fit to the formation energy of $L1_2$ Al_3Mg, along with other known ordered phases [22]. While the precipitation of ordered phases on dislocations in Al-Mg alloys has not, to our knowledge, been previously reported from experimental studies, the heterogeneous precipitation of $L1_2$ precipitates is known in other binary alloys. For example, the heterogeneous precipitation of $L1_2$ Al_3Li is well known in Al-Li alloys [34,35]. In the present case, the ordering occurs only in a small volume under the dislocation, but by lowering the temperature and allowing the ordering to go to completion it was found that the stoichiometric phase corresponds to $D7$ (Al_7Mg) [36]. This phase shares some similarities with an ordered $L1_2$ phase but has half the solute content. In particular, the Mg atoms alternate along [1$\bar{1}$0] and [$\bar{1}\bar{1}$2] directions as indicated by the unit cell in Fig. 9. A hint of such a tendency for ordering of Mg beneath an edge dislocation was pointed out in an earlier MC study using the same Al-Mg potential [12], but in that case the heavy computational cost of the MC simulations precluded full equilibration of the structure.

IV. CONCLUSION

Given the importance of solute-defect interactions, new techniques are required which allow us to bridge the gap between the atomic-scale energy landscape that determines the spatially varying equilibrium solute field and the diffusive time scales over which solute redistribution occurs. Traditionally, kinetic Monte Carlo simulations have allowed for coarse graining of time in atomistic simulations but such simulations become unreasonably burdened by the need to know all barriers for simulations involving solute-defect interactions, particularly in nondilute alloys where long-range interactions exist. In this paper, we have presented a version of the diffusive molecular dynamics (DMD) model parametrized to study binary alloys with previously developed, well-characterized EAM potentials. This technique is numerically stable and avoids issues related to vacancy condensation in the original version of the model.

To illustrate the potential of this technique, we examined segregation of solute atoms to two different defects in binary Al-Mg alloys. First, Mg segregation to an intrinsic stacking fault in fcc Al was simulated and the results compared to classical continuum models. In a second example, segregation of Mg driven by the long-range elastic strain field of a split edge dislocation was studied. As a further illustration of the potential of this technique, it was used to predict the

nucleation of an ordered phase below an edge dislocation, an effect only hinted at in previous MC simulations of the same system. This points to promising new avenues for studying atomic-scale phenomena over time scales relevant to practical problems where solute redistribution plays a fundamental role in determining properties of technological importance.

ACKNOWLEDGMENTS

We thank S. Sarkar for providing source code of the original DMD implementation [20] that served as a point of departure for this work. We also thank D. J. Srolovitz for many discussions. This work was supported by the Natural Sciences and Engineering Research Council of Canada.

[1] A. P. Sutton and R. W. Balluffi, *Interfaces in Crystalline Materials* (Oxford University Press, Oxford, UK, 1995).
[2] J. M. Howe, *Interfaces in Materials: Atomic Structure, Thermodynamics and Kinetics of Solid-Vapor, Solid-Liquid and Solid-Solid Interfaces* (Wiley, New York, 1997).
[3] C. Cui, L. Gan, M. Heggen, S. Rudi, and P. Strasser, Nat. Mater. **12**, 765 (2013).
[4] J. Cho, C. M. Wang, H. M. Chan, J. M. Rickman, and M. P. Harmer, Acta Mater. **47**, 4197 (1999).
[5] G. Duscher, M. F. Chisholm, U. Alber, and M. Rhle, Nat. Mater. **3**, 621 (2004).
[6] J. D. Baird, Metall. Rev. **16**, 1 (1971).
[7] Y. Estrin, L. P. Kubin, and E. C. Aifantis, Scr. Metall. Mater. **29**, 1147 (1993).
[8] S. I. Hong, Mater. Sci. Eng. **82**, 175 (1986).
[9] G. Horvath, N. Q. Chinh, J. Gubicza, and J. Lendvai, Mater. Sci. Eng., A **445–446**, 186 (2007).
[10] W. A. Curtin, D. L. Olmsted, and L. G. Hector, Nat. Mater. **5**, 875 (2006).
[11] Z. Xu and R. C. Picu, Modell. Simul. Mater. Sci. Eng. **14**, 195 (2006).
[12] D. Zhang and R. C. Picu, Modell. Simul. Mater. Sci. Eng. **12**, 121 (2004).
[13] D. Zhang and C. Picu, Int. J. Multiscale Computat. Eng. **7**, 475 (2009).
[14] D. Olmsted, L. Hectorjr, and W. Curtin, J. Mech. Phys. Solids **54**, 1763 (2006).
[15] F. Zhang and W. A. Curtin, Modell. Simul. Mater. Sci. Eng. **16**, 055006 (2008).
[16] D. McLean, *Grain Boundaries in Metals* (Clarendon, Oxford, 1957).
[17] S. M. Foiles, Phys. Rev. B **32**, 7685 (1985).
[18] R. LeSar, R. Najafabadi, and D. J. Srolovitz, Phys. Rev. Lett. **63**, 624 (1989).
[19] R. LeSar, R. Najafabadi, and D. J. Srolovitz, J. Chem. Phys. **95**, 6197 (1991).
[20] J. Li, S. Sarkar, W. T. Cox, T. J. Lenosky, E. Bitzek, and Y. Wang, Phys. Rev. B **84**, 054103 (2011).
[21] S. Sarkar, J. Li, W. T. Cox, E. Bitzek, T. J. Lenosky, and Y. Wang, Phys. Rev. B **86**, 014115 (2012).
[22] X. Y. Liu and J. B. Adams, Acta Mater. **46**, 3467 (1998).
[23] E. Brandes and G. Brook, *Smithells Metals Reference Book* (Butterworth-Heinemann, Oxford, 1992).
[24] N. Saunders, Calphad **14**, 61 (1990).
[25] A. R. Denton and N. W. Ashcroft, Phys. Rev. A **43**, 3161 (1991).
[26] H. H. Pham, M. E. Williams, P. Mahaffey, M. Radovic, R. Arroyave, and T. Cagin, Phys. Rev. B **84**, 064101 (2011).
[27] A. H. Cottrell and B. A. Bilby, Proc. Phys. Soc., London, Sect. A **62**, 49 (1949).
[28] N. Louat, Scr. Metall. **15**, 1167 (1981).
[29] R. W. Smith, R. Najafabadi, and D. J. Srolovitz, Acta Metall. Mater. **43**, 3621 (1995).
[30] T. Sato and A. Kamio, Mater. Sci. Eng., A **146**, 161 (1991).
[31] T. Sato, Y. Kojima, and T. Takahashi, Metall. Trans. A **13**, 1373 (1982).
[32] M. J. Starink and A.-M. Zahra, Philos. Mag. A **76**, 701 (1997).
[33] M. Slabanja and G. Wahnstrm, Acta Mater. **53**, 3721 (2005).
[34] Z. M. Wang and G. J. Shiflet, Metall. Mater. Trans. A **29**, 2073 (1998).
[35] Z. M. Wang and G. J. Shiflet, Metall. Mater. Trans. A **27**, 1599 (1996).
[36] Z. W. Lu, S.-H. Wei, A. Zunger, S. Frota-Pessoa, and L. G. Ferreira, Phys. Rev. B **44**, 512 (1991).